Mass Accommodation Coefficients of Phenol, 2-Nitrophenol, and 3-Methylphenol over the Temperature Range 278−298 K

B. Müller and M. R. Heal*

Department of Chemistry, University of Edinburgh, West Mains Road, Edinburgh, EH9 3JJ, U.K.

Received: September 17, 2001; In Final Form: March 12, 2002

The reactive uptake of phenol, 2-nitrophenol, and 3-methylphenol (*m*-cresol) was measured in a vertical wetted-wall flow reactor over the temperature range 278−298 K using bromine as an aqueous phase scavenger. First-order decays in gas-phase concentration as a function of increased gas−liquid contact time in the reactor were monitored by UV absorption downstream of the contact zone. Mass accommodation coefficients, α, were derived from measured uptake coefficients by correcting for limitations to mass transfer from radial gas-phase diffusion. Temperature-dependent expressions fitted to the data yielded values of α that decrease from 3.7×10^{-2} to 6.6×10^{-3} for phenol, 1.5×10^{-2} to 1.1×10^{-3} for 2-nitrophenol, and 1.0×10^{-2} to 5.1×10^{-3} for *m*-cresol over the range 278 K to 298 K. (Estimated overall uncertainty in α values of $\sim\pm 30\%$). These are the first published accommodation data for the latter two aromatic species. The thermodynamic data derived from the values of α were interpreted in terms of the critical cluster model for mass accommodation, yielding average critical cluster sizes of 3.2 ± 0.6, 4.1 ± 1.0, and 2 ± 0.5, for phenol, 2-nitrophenol, and *m*-cresol, respectively. The larger critical cluster size for 2-nitrophenol is likely attributable to its strong intramolecular hydrogen bonding which significantly reduces the hydrogen bonding strength of this species relative to the other two phenols. It is also demonstrated that the magnitude of the observed enthalpy of mass accommodation for these aromatic compounds correlates well with their excess energy of dissolution. The studied aromatic compounds are important intermediates in the tropospheric oxidation of monoaromatics and react readily in the aqueous phase. Thus knowledge of the mass accommodation coefficient is required to accurately quantify their rate of aqueous phase oxidation.

Introduction

Heterogeneous processes involving the liquid or solid condensed phase are acknowledged to have a highly significant role in the chemistry of both the troposphere and the stratosphere. For example, the presence of rain, cloud, and fog droplets can significantly affect the oxidative capacity of the troposphere by providing additional or alternative reaction pathways for trace atmospheric species.[1]

Since the bulk of the chemistry of the troposphere occurs on fairly rapid time scales it is not sufficient to describe heterogeneous interactions solely in terms of equilibrium thermodynamics. Instead, a quantitative understanding of the kinetics of molecular mass transport between, and within, the gas and aqueous phases is required. According to the kinetic theory of gases, the pseudo-first-order rate coefficient for the rate of loss of a species from the gas phase to the liquid phase is given by $(\gamma/4)\omega A_c$, where A_c is the surface area per unit volume of liquid phase, ω is the mean gas-phase molecular velocity, and γ is a net uptake coefficient that quantifies the overall probability of transfer from gas to liquid phases under the given conditions. A fundamental parameter within the expression for γ is the interfacial mass accommodation coefficient, α, which is defined as the fraction of collisions of the gas-phase species with the surface that results in incorporation of the species into the condensed phase. Values of α are required in atmospheric models to calculate the rate of condensed phase reactions. Laboratory studies of gas−liquid interactions are usually performed by bringing the gas and liquid into contact under precisely controlled conditions and measuring the loss of gas due to uptake by the liquid. In the past decade a wide range of experimental techniques have been developed for carrying out such uptake measurements and mass accommodation coefficients have been measured for trace gases such as SO_2, H_2O_2, O_3, NO_2, $ClNO_2$, HNO_3, and aliphatic alcohols and acids.[2−7]

The oxidizing capacity of the troposphere and the fate of volatile organic compounds (VOC) emitted to the atmosphere are intimately entwined. One important class of such compounds are the monoaromatic compounds; typical gasoline blends have an aromatic content of 20−30 vol %.[8] Various laboratory studies have demonstrated that the gas-phase oxidation of aromatic compounds such as benzene and toluene, by OH and NO_3 radicals, leads to phenol and mono- and dinitro-substituted phenols. However, the fate of these compounds with respect to the aqueous phase, i.e., the uptake of the gaseous species and subsequent reactions in the liquid phase, are less well understood. Only recently have laboratory studies of aromatic compounds with free radicals in the aqueous phase been carried out.[9−13] Measured rate coefficients for reactions in the aqueous phase are much larger (e.g., ~5 orders of magnitude for reaction of benzene with NO_3) than the equivalent reaction in the gas phase.[9] This suggests an important atmospheric pathway for aromatic compounds that may compete with gas-phase reactions. Furthermore, hydroxy- and nitro-substituted ring-retaining products of gas-phase aromatic oxidation, which are more water-soluble than the precursor hydrocarbons, can transport into the aqueous phase and undergo further reactions.[14] In addition to the importance for the fate of the aromatic compounds, the

* Corresponding author. Fax: (+44) 131 650 4743. E-mail: m.heal@ed.ac.uk.

10.1021/jp013559+ CCC: $22.00
Published on Web 04/25/2002

aqueous phase reactions between aromatic compounds and free radicals may also significantly influence the free radical budget in the aqueous phase and alter the oxidizing strength of the aqueous medium.

At present, data are virtually nonexistent with respect to accommodation of aromatic compounds into the aqueous phase. Heal et al.[15] have previously measured the mass accommodation coefficients of phenol, toluene, and aniline using the droplet train technique. Here, we measure the accommodation of phenol, 2-nitrophenol, and 3-methylphenol (*m*-cresol) over a tropospherically relevant temperature range, using a wetted-wall flow reactor. Phenols and nitrophenols have been identified in rain, snow, surface water, and fog, as well as in air samples, at concentrations exceeding those which can be accounted for by primary emission.[16−24] The phytotoxic properties of some nitrophenols has also led to the proposal that they could be one contributor to forest decline.[25] The reactions leading to nitrophenol formation (in either the gas or liquid phases) impacts upon the distribution of NO_y species in the troposphere.[26,27] Mass accommodation coefficients are required to help elucidate the atmospheric source and fate of these important environmental species.

Formulation and Measurement of Gas−Liquid Uptake

The net transfer of a gas into a liquid is the result of a series of processes: gas-phase diffusion to the surface, mass accommodation, Henry's law solubility, liquid-phase diffusion, and liquid-phase reaction. Since these processes do not occur in isolation, the overall gas−liquid mass transfer is described mathematically by coupled differential equations. Only for limited cases can exact solutions be found.[28] In the resistance model of gas−liquid mass transfer, the resistance to mass transfer of each of the processes is considered independently of each other to obtain a simple approximation based on steady-state solutions. The resulting equation expresses the observed net gas-to-liquid uptake coefficient, γ, in terms of the contribution of the resistances of the individual processes to the overall uptake resistance, $1/\gamma$, [29]

$$\frac{1}{\gamma} = \frac{1}{\Gamma_G} + \frac{1}{\alpha} + \frac{1}{\Gamma_{SOL} + \Gamma_{RXN}} \quad (1)$$

By continued analogy to the terminology of an electric circuit, α is the conductance due to interfacial transfer, and the Γ_G, Γ_{SOL}, and Γ_{RXN} functions are the conductances (dimensionless mass transfer coefficients) for gas-phase diffusion, Henry's law saturation, and liquid-phase reaction, respectively. The individual conductances can be expressed explicitly using gas kinetic theory appropriate to the geometry under consideration.[29,30]

Gas diffusion:
$$\Gamma_G = \frac{2(3.66D_G)}{\omega r}$$
(for cylindrical flow-reactor geometry) (2)

Liquid solubility:
$$\Gamma_{SOL} = \frac{4HRT}{\pi^{1/2}\omega}\sqrt{\frac{D_L}{t}} \quad (3)$$

Liquid reaction:
$$\Gamma_{RXN} = \frac{4HRT\sqrt{D_L k_{RXN}}}{\omega} \quad (4)$$

In eqs 2−4, $\omega = \sqrt{8kT/\pi m}$ (where m is the molecular mass) is the mean molecular velocity of the trace species in the gas phase, D_G is the gas diffusion coefficient, r is the radius of the flow reactor, H is the Henry's law coefficient, T is the temperature, t is the liquid−gas contact time, D_L is the liquid diffusion coefficient, and $k_{RXN} = k''$ [X] is the pseudo-first-order rate coefficient for a second-order reaction with rate coefficient k'' between the transferred species and a reactant X in the liquid.

In experiments to measure α it is useful to arrange conditions so that its value can be extracted more directly from eq 1. By adding an efficient chemical scavenger for the trace species it is possible to ensure that the total liquid-phase resistance, $1/(\Gamma_{SOL} + \Gamma_{RXN})$, is negligible in comparison with the interfacial resistance due to gas diffusion and mass accommodation, $(1/\alpha + 1/\Gamma_G)$. In this work, bromine was added as the scavenger for the phenols on aqueous surfaces.

Experimental Section

Wetted-Wall Flow Reactor. Uptake coefficients were measured using a vertical wetted-wall flow reactor, constructed of Pyrex glass, 90 cm long, and with an internal diameter of 1.6 cm. The experimental setup was similar to that described by Utter et al.[4] and a schematic diagram is shown in Figure 1. A thin aqueous film flowed continuously down the internal walls of the reactor. A gas stream entrained with the trace species of interest flowed along the center of the reactor at subambient pressure. This experimental method has the advantages that the liquid surface is constantly renewed, so the composition of the liquid film remains essentially constant, and that mass transport theory for cylindrical flow can be applied to the data analysis.

To maintain a constant experimental temperature the flow tube was surrounded by a glass jacket containing ethylene glycol as a coolant fluid. A recirculating chiller (Cole-Parmer, Polystat) pumped the coolant through the jacket and also through two further glass coiled heat exchangers to pre-cool the aqueous solution and the carrier gas prior to their entry into the flow tube. All aqueous flow lines consisted of $^1/_4$-in. nylon tubing which were jacketed by foamed rubber tubing for temperature insulation.

The water used to make aqueous solutions was deionized to a resistance of 10 MΩ. The aqueous solution was pumped into the top of the reactor from a 6 L storage tank above the flow tube using a liquid pump (L/S Masterflex). A pulse dampener (Cole Parmer) was fitted into the line to eliminate pulses in the liquid flow. After passing through the heat exchanger the liquid filled a small annular collecting reservoir in the upper part of the flow tube. The solution spilled over the lip of the retaining wall of the reservoir to form a thin film of downward flowing liquid, uniformly wetting the entire inner surface of the flow tube. At the bottom of the reactor assembly the solution collected into a 6 L flask, which was cooled to about −15 °C by an ice−salt mixture in order to prevent back-streaming of water vapor into the flow tube.

It was necessary to clean the inner surface of the flow tube regularly to ensure uniform wetting. This was done by washing with detergent, followed by thorough rinsing with deionized water.

The trace gas of interest, entrained in a flow of He, entered the reactor through a movable glass injector with an inner diameter of 3 mm. Different exposure times between trace gas and liquid surface (the gas−liquid contact time, t') were achieved by varying the injector position. A rigid injector holder ensured the central alignment of the injector within the flow tube.

The main flow of He carrier gas entered the reactor at a sidearm above the wetted film. The gas was humidified before entering the reactor to avoid evaporative cooling of the liquid

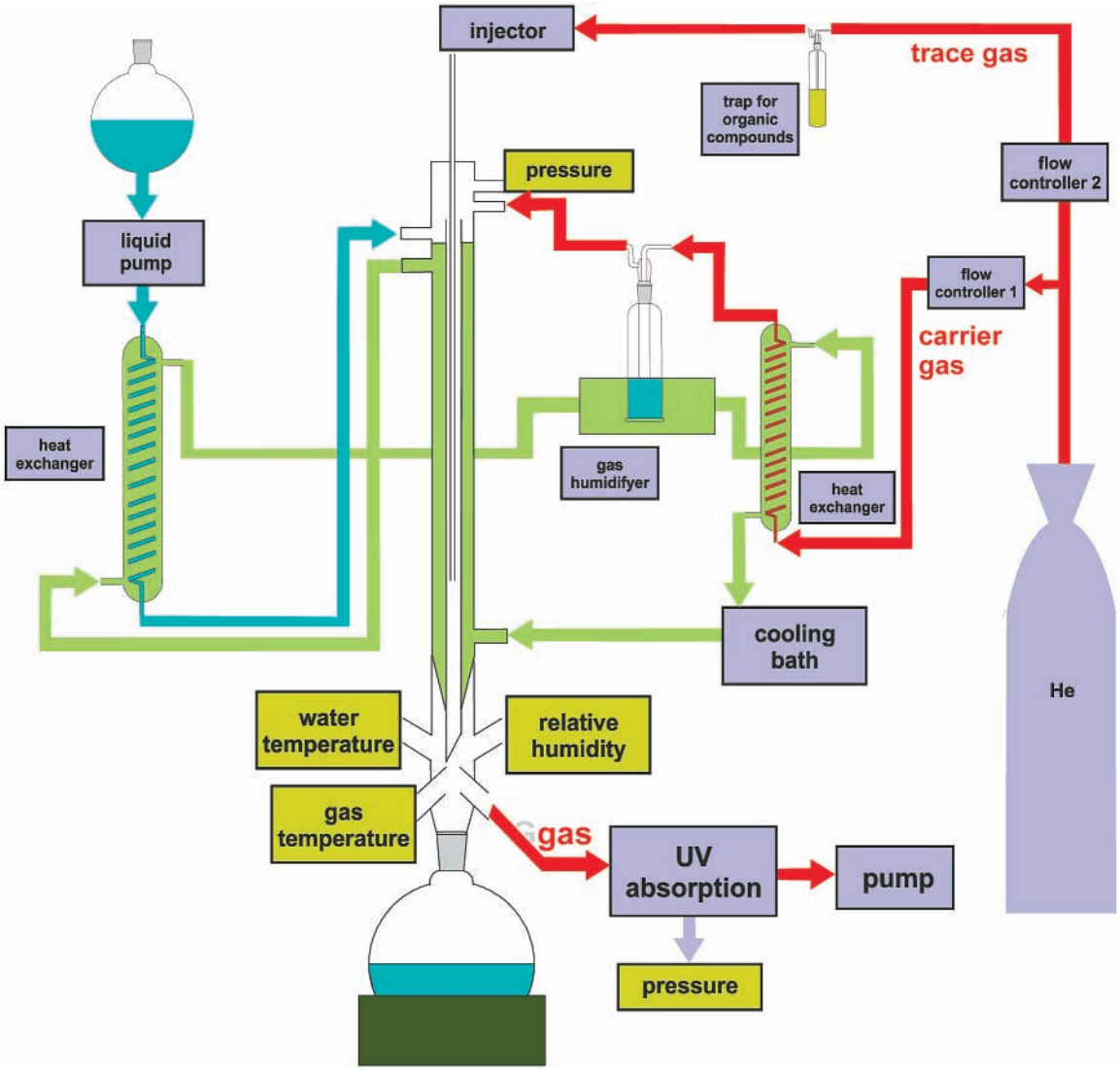

Figure 1. Schematic diagram of the wetted-wall flow reactor system.

film and to maintain a well-defined temperature in the reactor. Humidification was achieved by passing the gas through a thermostatically controlled water bubbler containing deionized water. The relative humidity in the flow reactor was measured using a humidity meter (Vaisala, HMP 234).

Experiments were performed in the temperature range 278−298 K. The temperature of the flowing liquid and the gas were checked by inserting thermocouples (type K) into the bottom of the reactor. The gas temperature measured by the thermocouple could be corroborated against the temperature reading at the humidity meter.

The flow reactor was operated at low pressures, typically in the range 10−100 Torr, monitored using two capacitance manometers (Edwards, Barocel 600AB) with 0−100 and 0−1000 Torr scales. Pressure within the system was measured at the top of the flow tube as well as at the UV cell. The partial pressure of water vapor, p_{H_2O}, was determined from the humidity measurements, and the partial pressure of He, p_{He}, by subtraction of p_{H_2O} from total reactor pressure, p. The partial pressure of trace species, i, was assumed negligible.

Gas flow rates were regulated by calibrated electronic mass flow controllers (Tylan, FC 280 SA; control box RO-28). The total gas flow was varied in the range of 0.3−3 L min^{-1} (STP) which corresponded to linear gas velocities of 50−2000 cm s^{-1} under the experimental conditions used.

Although the reactor had a maximum gas−liquid contact length of 80 cm, the first 12 cm region was not used in order to allow laminar gas flow to establish and water vapor to saturate the He stream. The remaining 68 cm of interaction zone typically led to contact times of gas with liquid surface in the range 0.03−0.3 s. For comparison, contact times of the liquid surface with gas ranged between 0.5 and 5.0 s, depending on particular combinations of water and gas flow rates.

UV Absorption Detection. Changes in trace gas concentrations following exposure to the aqueous surface were measured using wavelength-resolved UV absorption spectroscopy. The gas exited the wetted-wall flow reactor through a sidearm beneath the aqueous surface and passed through a 90 cm long cylindrical gas cell made of Pyrex glass with quartz windows (U. Q. G., Spectrosil B).

The collimated UV light from a 150 W Xe lamp (Osram, XBO) passed first through an iris, then the gas cell, and was focused on to the entrance slit (10 μm) of an f/4 grating spectrometer (Instrument SA, 270M Rapid Scanning Imaging Spectrograph) of focal length 270 mm. The light was dispersed by a 300 groove mm^{-1} grating with a 250 nm blaze, covering a wavelength range from about 170 to 500 nm. The dispersed light was detected with a 1024 element photodiode array (Instrument SA, QuikScan) of total area 25.6 mm × 2.5 mm. Spectral wavelength resolution was about 0.9 nm for a grating

dispersion of approximately 12.4 nm mm^{-1}. Integrated software (Instrument SA, SpectraMax) controlled the spectrograph and the data acquisition. Values of absorption were measured at the wavelength of maximum absorption cross-section in the region 250−300 nm. For example, for phenol, $\sigma = 2.5 \times 10^{-17}$ cm^2 at $\lambda = 269$ nm.[31] The absorption cross-section of gaseous Br_2 is more than 4 orders of magnitude smaller at this wavelength.[32] Changes in gas-phase aromatic absorption were referenced against a background absorption not containing the aromatic species.

Chemicals. The aromatic compounds investigated are in a condensed physical state at the temperatures at which the experiments were performed. Crystalline phenols (BDH, >99%) were ground in a mortar and transferred to a small 10 cm trap upstream of the flow reactor. He for the trace gas flow passed through this trap via a sintered disk in order to maintain a direct contact between the gas and the aromatic compound. This approach was found to provide a continuous and constant concentration of trace gas entrained in the helium gas flow. Measurements of trace gas absorption spectra indicated that trace gas concentrations were typically in the range $(0.5-1) \times 10^{14}$ molecules cm^{-3}.

The bromine solution used as the liquid-phase scavenger for the phenols was prepared by adding ~1 mL of bromine (Fisher, >99%) into 2.5 L of deionized water and stirring overnight. The solution was then transferred to the reservoir tank above the flow reactor.

Data Analysis and Results

Phenols undergo facile electrophilic substitution with bromine in solution. Thus, the addition of bromine to the liquid phase enhances the uptake rate by maintaining a flux of the trace gas across the interface. In terms of the individual resistances expressed in eq 1, the effect of the scavenger is to make the resistance term $(\Gamma_{SOL} + \Gamma_{RXN})^{-1}$ arising from the liquid-side transfer negligible (through a large value for k_{RXN} in Γ_{RXN}) in comparison with the resistance to uptake due to gas diffusion and mass accommodation.

Bell and Rawlinson[33] have measured the rate coefficient for the reaction of phenol with bromine as 1.8×10^5 M^{-1} s^{-1} at 298 K, although they acknowledge a low accuracy for this value since the reaction between phenol and bromine in aqueous solution is very fast. A more recent value for the rate coefficient, also at 298 K, has been given by Tee et al.[34] These workers report that the reaction is first order in each reactant with a pH-dependent rate coefficient calculated from $k'' = k_1 + k_2 K_A/[H^+]$, where k_1 and k_2 are the rate coefficients for the reaction of undissociated phenol and phenoxide ion ($C_6H_5O^-$) with bromine, respectively. The values of $k_1 = 4.3 \times 10^5$ M^{-1} s^{-1} and $k_2 = \sim 1.2 \times 10^9$ M^{-1} s^{-1} given by Tee et al.[34] were used to calculate $k'' = 1.98 \times 10^6$ M^{-1} s^{-1} for pH = 7. (A value of $pK_A = 9.89$ for the phenol acid dissociation constant at 298 K was used[35]).

The aqueous phase concentration of bromine in the wetted film was estimated to be about 0.01 M using a ρ_{Br_2} of 3.1 g cm^3 at 293 K.[35] This leads to a value for k_{RXN} of 2×10^4 s^{-1} using $k'' = 1.98 \times 10^6$ M^{-1} s^{-1}. Values of $k_{RXN} = 5 \times 10^6$ s^{-1} and $k_{RXN} = 1 \times 10^4$ s^{-1} were likewise calculated for the reactions of 2-nitrophenol and *m*-cresol, respectively, with the bromine scavenger.[34]

Using these values, and other parameters appropriate to the experimental conditions, it is easy to show from eqs 1−4 that the liquid uptake resistance from solubility and reaction, $(\Gamma_{SOL} + \Gamma_{RXN})^{-1}$, is very small compared with the combined resistance due to gas diffusion to the surface and mass accommodation. For example, using data for typical experiments with phenol at 293 K ($H = 4300$ M atm^{-1},[36] $\omega = 2.56 \times 10^4$ cm s^{-1}, $D_G = 2.5$ cm^2 s^{-1} (see later), $D_L = 9.2 \times 10^{-6}$ cm^2 s^{-1} (calculated using the Wilke-Chang method[37]), $t = 2$ s, and $k_{RXN} = 2 \times 10^4$ s^{-1}), the term $(\Gamma_{SOL} + \Gamma_{RXN})^{-1} = (7 + 0.02)^{-1} \approx 0.1$. (Published values of H for phenols vary widely. Consequently this group have undertaken new experimental determinations for use in this work. For example also, H (293 K) = 121 M atm^{-1} for 2-nitrophenol[36]). Since, by definition, α cannot exceed unity, the maximum the term $(\Gamma_{SOL} + \Gamma_{RXN})^{-1}$ can contribute to the observed uptake resistance, $1/\gamma$, in eq 1 is 10%. For anticipated values of $\alpha < 0.1$, the maximum contribution of liquid-phase resistance to overall uptake resistance is less than 1%. Therefore, the aqueous concentration of bromine is not important as long as it is sufficient to ensure that the term containing $1/\Gamma_{RXN}$ in eq 1 has a negligible contribution to overall mass transfer.

Under these experimental conditions, eq 1 reduces simply to,

$$\frac{1}{\gamma} = \frac{1}{\alpha} + \frac{\omega r}{7.32 D_G} \tag{5}$$

In other words, to a very good approximation, the mass accommodation coefficient is equal to the observed uptake coefficient corrected for limitations to mass transfer arising from diffusion of the trace species, *i*, in the gas phase to the wetted wall of the cylindrical reactor. When uptake of *i* into the liquid is large, gas-phase diffusion limitation leads to a radial concentration gradient of *i* and this correction term becomes significant. The experiments were conducted at relatively low pressure in order to reduce the magnitude of this correction as far as practicable.

In cylindrical geometry, the observed first-order rate coefficient, k_w, for loss from the gas phase is related to the uptake coefficient through,

$$\gamma = \frac{2 r k_w}{\omega} \tag{6}$$

Values of k_w were derived from the first-order decline in gas-phase concentration of *i* with increasing gas−liquid contact time, t',

$$\frac{d[i]}{dt'} = -k_w[i] \tag{7}$$

In practice, this means that values of k_w were obtained from gradients of plots of ln absorbance against injector position, converting injector position to gas−liquid contact time using the gas flow velocity calculated for the pressure/temperature conditions. An example k_w plot is shown in Figure 2. The uptake and mass accommodation coefficients corresponding to each k_w were derived from sequential application of eqs 6 and 5 as described above. The value of the gas diffusion coefficient, D_G, appropriate to each experiment was calculated from the equation,

$$\frac{1}{D_G} = \frac{p_{H_2O}}{D^P_{G(i-H_2O)}} + \frac{p_{He}}{D^P_{G(i-He)}} \tag{8}$$

where p_{H_2O} and p_{He}were the partial pressures of water and helium, respectively, in the reactor for that experimental run,

TABLE 1: Pressure-Independent Binary Gas Diffusion Coefficients for Trace Gas, *i*, in H_2O and He, as a Function of Temperature, Calculated from the Method of Fuller et al.[37] [a]

	phenol		2-nitrophenol		*m*-cresol	
T/K	$D^P_{G(i-H_2O)}$/ Torr cm^2 s^{-1}	$D^P_{G(i-He)}$/ Torr cm^2 s^{-1}	$D^P_{G(i-H_2O)}$/ Torr cm^2 s^{-1}	$D^P_{G(i-He)}$/ Torr cm^2 s^{-1}	$D^P_{G(i-H_2O)}$/ Torr cm^2 s^{-1}	$D^P_{G(i-He)}$/ Torr cm^2 s^{-1}
278	76.5	205.1	69.9	189.3	69.4	184.9
283			72.1	195.3		
288	81.4	218.2	74.4	201.4	73.8	196.7
293	83.9	224.9	76.7	207.6	76.1	202.7
298	86.4	231.6				

[a] The quoted significant figures do not represent the presumed precision in the method.

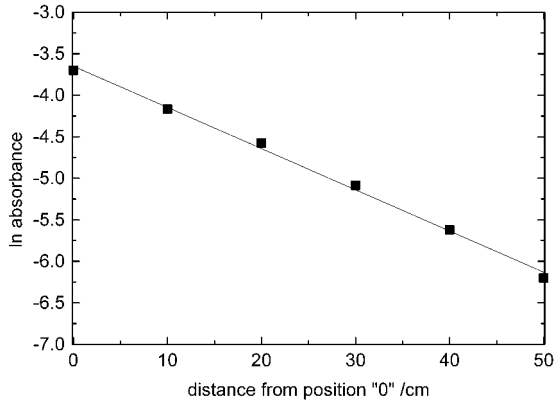

Figure 2. Plot of ln absorbance vs injector position for uptake of phenol onto bromine water at 293 K and with a gas velocity of $c = 251$ cm s^{-1}. The gradient gives $-k_w$.

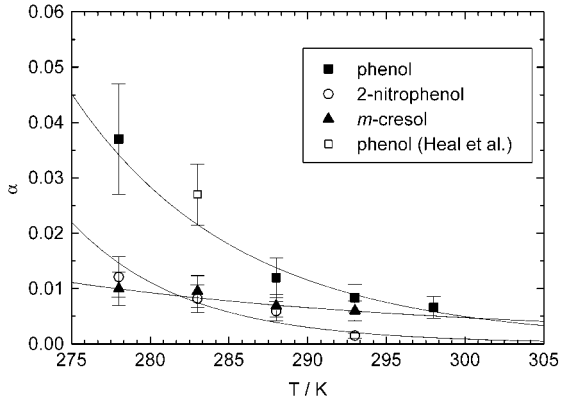

Figure 3. Mass accommodation coefficients of phenol, 2-nitrophenol, and *m*-cresol measured in this work as a function of temperature. Error bars are ±30% as discussed in the text. The solid lines correspond to the fits of eq 9 to the data as shown in Figure 4. Also shown is the single datum for phenol from Heal et al.[15] (open square).

TABLE 2: Mass Accommodation Coefficients of Phenol, 2-Nitrophenol, and *m*-Cresol at Different Temperatures[a]

	α		
T/K	phenol	2-nitrophenol	*m*-cresol
278	3.7×10^{-2}	1.2×10^{-2}	1.0×10^{-2}
283		8.2×10^{-3}	
288	1.2×10^{-2}	5.9×10^{-3}	6.9×10^{-3}
293	8.3×10^{-3}	1.5×10^{-3}	6.0×10^{-3}
298	6.6×10^{-3}		

[a] Estimated uncertainty in each value is ±30%.

and $D^P_{G(i-H_2O)}$ and $D^P_{G(i-He)}$ are the pressure-independent binary diffusion coefficients of *i* in H_2O and He, respectively. These latter coefficients were estimated using the molecular diffusion volume method of Fuller, Schettler, and Giddings.[37] The calculated values used are given in Table 1.

The uptake of the phenols on bromine water were measured in the temperature range 278−298 K. The resulting mass accommodation coefficients are given in Table 2. Each value of α is an average of at least five experimental runs with different observed first-order loss coefficients, k_w, obtained at different pressures. Each value of k_w is derived from absorbance measurements at six injector positions. A plot of the mass accommodation coefficients as a function of temperature for both compounds is shown in Figure 3.

There are a number of potential sources of error in determining γ and α. It is essential that the inside of the wall is wetted uniformly. Experiments were performed only when the wall was observed to be completely wetted. Ripples in the surface were apparent for water flow rates in excess of 150 mL min^{-1} and this can lead to enhanced mass transport in the liquid.[38] These high flow rates were therefore avoided.

Uncertainty in relative humidity during an experiment will lead to uncertainty in derived uptake data since the calculation of the gas flow velocity and the gas diffusion coefficients rely on exact control of the humidity in the flow reactor. Relative humidity is a strong function of temperature so temperature needs to be accurately controlled and maintained. Humidity was measured continuously at one point within the flow tube, and temperature at two points. Nevertheless, a realistic estimate of error in γ due to the effect of uncertainties and variation in humidity is probably ±20%. There is also likely to be uncertainty intrinsic to the empirical relationship used to derive the binary gas diffusion coefficients for correcting γ to give α. Assuming this error amounts to approximately a further ±20% (as discussed by Reid et al.[37]), and that uncertainty arising from determination of relative trace gas concentration by UV absorbance (for example, from random fluctuations in UV output) is ±5% to ±10%, then a realistic estimate for overall uncertainty in α is ∼±30%. These error ranges are indicated in Figure 3.

Discussion

The measured values for the mass accommodation coefficient of phenol range from 3.7×10^{-2} at 278 K to 6.6×10^{-3} at 298 K. The expected negative temperature dependence in α is clear (Figure 3). The single mass accommodation value of $\alpha = (2.7 \pm 0.5) \times 10^{-2}$ for phenol at 283 K published by Heal et al.[15] using a droplet train apparatus (also shown in Figure 3) fits the temperature trend measured in this work.

The mass accommodation coefficient of 2-nitrophenol is smaller than that of phenol, as shown in Figure 3, and its temperature dependence stronger. On the other hand, the temperature dependence in α for *m*-cresol is weaker than for phenol There are no previously reported measurements of α for 2-nitrophenol or *m*-cresol, nor for any other phenol or nitro-containing compound for comparison. The only other literature mass accommodation coefficient for a substituted aromatic

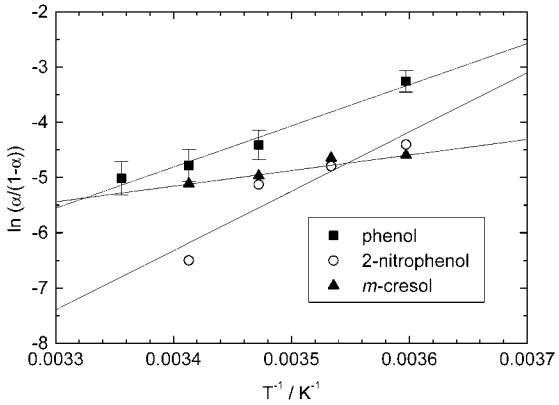

Figure 4. Plot of $\ln(\alpha/(1-\alpha))$ against $1/T$ for phenol, 2-nitrophenol, and *m*-cresol. The estimated error ranges shown in Figure 3 are plotted here as an example for phenol only.

TABLE 3: Values of Enthalpy and Entropy Associated with Mass Accommodation for Phenol, 2-Nitrophenol, and *m*-Cresol[a]

	ΔH_{obs}/kJ mol^{-1}	ΔS_{obs}/J mol^{-1} K^{-1}
phenol	-62 ± 8	-250 ± 25
2-nitrophenol	-89 ± 25	-354 ± 86
m-cresol	-24 ± 2	-123 ± 4

[a] Quoted errors represent only ± 1 standard deviation of error in the linear regression fits shown in Figure 4.

compound (other than phenol) is a single value of $\alpha = (1.8 \pm 0.5) \times 10^{-2}$ at 283 K for the amino-substituted mono-aromatic, aniline.[15]

It can be noted that since all derived values of α are less than 4×10^{-2}, the assumption in the previous section that liquid-phase resistance is negligible in comparison to interfacial resistance is entirely justified.

By consideration of the transition state between gas and solvated state, Davidovits and co-workers have formulated the following relationship between α and the observed Gibbs free energy, ΔG_{obs}, for accommodation,[39,40]

$$\ln\left(\frac{\alpha}{1-\alpha}\right) = -\frac{\Delta G_{obs}}{RT} = -\frac{(\Delta H_{obs} - T\Delta S_{obs})}{RT} \qquad (9)$$

The associated enthalpy ΔH_{obs} and entropy ΔS_{obs} for accommodation are derived from the slope and intercept, respectively, of a plot of $\ln(\alpha/(1-\alpha))$ against $1/T$. Such a plot is shown in Figure 4 for the data obtained here. The resulting thermodynamic parameters are tabulated in Table 3. The fitted lines in Figure 4 yield the following relationships for deriving values of α as a function of temperature (illustrated also in Figure 3):

phenol: $$\alpha = \left(\exp\left(-\frac{7440}{T} + 30.1\right) + 1\right)^{-1}$$

2-nitrophenol: $$\alpha = \left(\exp\left(-\frac{10700}{T} + 42.7\right) + 1\right)^{-1}$$

m-cresol: $$\alpha = \left(\exp\left(-\frac{2830}{T} + 14.8\right) + 1\right)^{-1}$$

There are no previous literature thermodynamic parameters for aromatic accommodation coefficients against which to compare.

It remains a matter to try and rationalize observed trends in values of ΔH_{obs} for mass accommodation of different compounds into aqueous surfaces. The previous cavity model of gas uptake[41] predicted a direct relation between the hydrogen-bonding ability of species of comparable size and ΔH_{obs}, whereas Davidovits et al.[3] observed an inverse correlation for aliphatic alcohols and acids, in which species with presumed greater hydrogen-bonding tendency (for example, diols) were associated with less negative values of ΔH_{obs}. In response, these latter workers have formulated a critical cluster nucleation model of gas uptake to try and interpret the thermodynamics of observed mass accommodation coefficients.[39,40] In this model it is suggested that uptake is controlled by the aggregation of water molecules (solvent) around the incoming trace gas molecule at the interface. The interface itself is viewed as a dynamic region where these aggregates (clusters) continually form, fall apart, and reform. A cluster is composed of N molecules, which is the sum of the trace gas molecule and the surrounding water molecules. Clusters smaller than some critical size N^* fall apart, whereas clusters larger than N^* serve as centers for further condensation and grow in size until they merge into the bulk liquid.

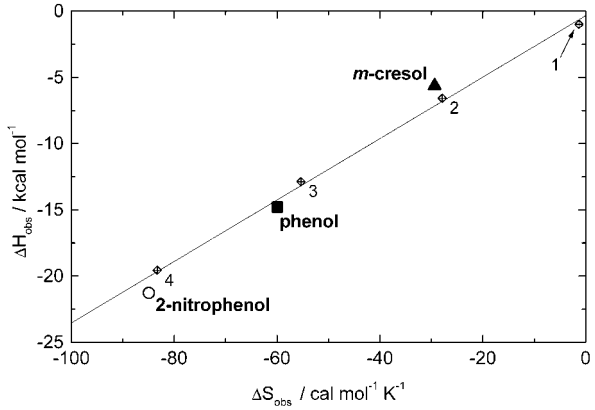

Figure 5. Plot of ΔH_{obs} against ΔS_{obs} for phenol, 2-nitrophenol, and *m*-cresol. The solid line connects calculated values of ΔH_{obs} and ΔS_{obs} according to the model by Davidovits et al.[40,42] The numbers refer to the critical number N^* in this model.

The equilibrium density of clusters at the surface is proportional to the molar free energy $\Delta G_{obs} = \Delta H_{obs} - T\Delta S_{obs}$ for the formation of a cluster of N molecules. On the basis of experimental data mainly for aliphatic alcohols, haloethanols, and aliphatic acids, Davidovits et al.[40] and Nathanson et al.[42] have provided expressions to calculate ΔH_{obs} and ΔS_{obs} for selected values of N^*. These are plotted in Figure 5, together with the experimental data obtained in this work for phenol, 2-nitrophenol, and *m*-cresol.

It is interesting to note from Figure 5 that the relative values of ΔH_{obs} and ΔS_{obs} for the phenols studied here follow the same linear relationship derived in the critical cluster model from the data for the aliphatic alcohols. Applying the formulas for ΔH_{obs} and ΔS_{obs} given by Nathanson et al.,[42] the measured values of ΔH_{obs} and ΔS_{obs} correspond to values of $N^* \approx 3.2$, ≈ 4.1, and ≈ 2 for the critical sizes of cluster for phenol, 2-nitrophenol, and *m*-cresol, respectively, in the mass accommodation process. Carrying through the estimated overall uncertainties in α discussed above (illustrated as error bars in Figure 4) yields corresponding estimates of uncertainty in the derived values of N^* of ± 0.6, ± 1, and ± 0.5.

The critical number N^* is assumed to represent a measure of how readily a molecule is incorporated into the bulk liquid. Davidovits et al.[40] postulated that the number N^* required to form a critical cluster depends on the structure of the specific molecule undergoing the uptake process. They further proposed that the ease with which the cluster is formed is determined primarily by the number of hydrophilic functional groups, and

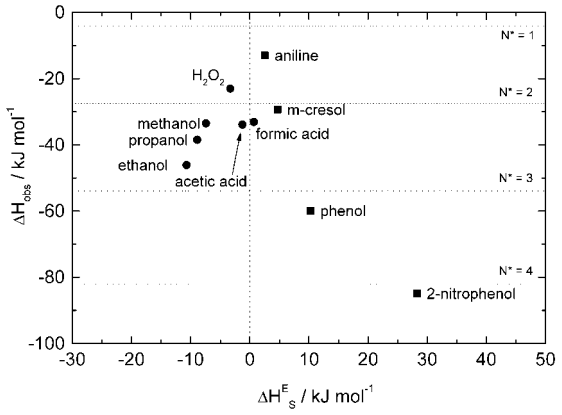

Figure 6. Plot of ΔH_{obs} against excess enthalpy of solution, ΔH_S^E. Values of ΔH_{obs} for phenol, 2-nitrophenol, and *m*-cresol were measured in this work, while ΔH_{obs} for aniline is that reported by Titcombe.[49] Values of ΔH_S^E for the aromatic compounds were estimated from a plot of ln(solubility) vs $1/T$;[48,53] solubility values were taken from Landolt-Börnstein *Physikalisch-Chemische Tabellen*.[54] Values of ΔH_{obs} for aliphatic compounds (circles) were taken from Davidovits et al.[40] and of ΔH_S^E from Schwarzenbach et al.[48] and Maskill.[47] All data refer to room temperature. The lines of N^* are based on values of ΔH_{obs}.

that once the critical cluster is formed around the hydrophilic part, the cluster continues to grow independently of the size of the hydrophobic portion of the molecule. The argument is that a greater hydrogen-bonding capability in the incoming molecule requires less additional water molecules to bind to it to form the critical cluster. Thus species with more hydrogen-bonding functional groups give rise to less negative values of ΔH_{obs}. However, although this model successfully addresses many general observations regarding values of ΔH_{obs}, it remains the case that values of ΔH_{obs} for individual species cannot yet be accurately predicted in advance. Thus, no attempt has been made to correlate ΔH_{obs} directly with the effective hydrogen bond acidity of the incoming solute, or indeed with combinations of other possibly relevant solute−solvent interaction parameters such as the solute effective hydrogen bond basicity, the solute polarizability, or the solute characteristic volume.[43] For the aromatics species studied here, it can be noted that strong intramolecular hydrogen-bonding within 2-nitrophenol considerably reduces the magnitude of its hydrogen-bonding acidity in comparison with phenol and *m*-cresol,[44] which likely explains the larger $-\Delta H_{obs}$ of the former. It should be noted, however, that the critical cluster approach is only one model for accommodation at the surface. Molecular dynamic simulation methods have been applied to the accommodation of ethanol and ethylene glycol on water surfaces[45,46] and predict lower barriers to solvation and larger accommodation coefficients for these species than experimentally determined.

As an alternative approach we examine the relationship between ΔH_{obs} and the excess enthalpy of dissolution, ΔH_S^E. This latter enthalpy is a measure of the interaction between solute and solvent. A negative (exothermic) value of ΔH_S^E indicates attraction between solute and solvent, associated with a high degree of solubility, whereas endothermic values of ΔH_S^E often reflect low solubilities. Values of ΔH_{obs} are plotted against known and estimated values of ΔH_S^E [47,48] in Figure 6. (The figure also includes the datum for aniline, as reported by Titcombe[49]). Only limited data regarding ΔH_{obs} for the aliphatic alcohols are available which makes it difficult to conclude general trends. All values of ΔH_{obs} are negative, but there are distinct differences in the values of ΔH_S^E. The three short-chain aliphatic alcohols for which both ΔH_S^E and α values are known have negative values of ΔH_S^E.

The aromatic compounds on the other hand show positive values of ΔH_S^E, and there appears to be a fairly strong relationship between ΔH_S^E and ΔH_{obs} for these compounds. 2-nitrophenol has the largest value of ΔH_S^E, i.e., relatively more energy is needed to dissolve it. It therefore seems reasonable that accommodation of 2-nitrophenol should demonstrate the greatest temperature dependence and consequently have the highest ΔH_{obs}, and hence highest critical cluster number N^*, of the aromatics studied. Although ΔH_S^E and ΔH_{obs} data are not both available for other aliphatic alcohols, there is a general trend for ΔH_S^E to increase with increasing chain length, e.g. $\Delta H_S^E = +0.5$ kJ mol^{-1} for octanol and $\Delta H_S^E = +10.7$ kJ mol^{-1} for dodecanol.[48] It will be instructive to determine whether the temperature dependence in α for such compounds fits the relationship with ΔH_S^E observed for the phenols.

A value of $\alpha < \sim 10^{-2}$ is the value at which mass accommodation rather than gas-phase diffusion, becomes the limiting factor to interfacial mass transfer to typical sized aqueous droplets in the atmosphere.[50] The mass accommodation coefficients reported here are thus in the α-limited regime for $T > \sim 280$ K for 2-nitrophenol and *m*-cresol and $T > \sim 290$ K for phenol. If there is no chemical reaction in the aqueous phase, the exact value of α is not particularly important since the concentration of the solute fairly rapidly reaches Henry's Law equilibrium, and no further net transfer from gas to liquid takes place. However, the atmospheric aqueous phase reactions of the aromatics investigated here are, or are likely to be, fast. Therefore their relative fate with respect to gas and aqueous phases needs to be modeled explicitly as a kinetic process for which values of α (as a function of temperature) are required. For example, Buxton et al.[51] report a rate coefficient of 1.8×10^{10} l mol^{-1} s^{-1} for reaction between phenol and OH, while Herrman et al.[9] give a rate coefficient of 8.4×10^8 L mol^{-1} s^{-1} for reaction between *p*-cresol and NO_3. Using estimated aqueous phase concentrations of 6×10^{-13} mol L^{-1} for OH[1] and 10^{-12} mol L^{-1} for NO_3[52] yields pseudo-first-order reaction rate constants of ~ 0.01 s^{-1} for both reactions. These are certainly large enough for rates of heterogeneous processes (i.e., the combined effect of interfacial transfer and aqueous reaction) to compete with rates of gas-phase reactions of the aromatics with OH and NO_3.

References and Notes

(1) Lelieveld, J.; Crutzen, P. J. *Nature* **1990**, *343*, 227−233.
(2) Worsnop, D. R.; Zahniser, M. S.; Kolb, C. E.; Gardner, J. A.; Watson, L. R.; Van Doren, J. M.; Jayne, J. T.; Davidovits, P. *J. Phys. Chem.* **1989**, *93*, 1159−1172.
(3) Jayne, J. T.; Duan, S. X.; Davidovits, P.; Worsnop, D. R.; Zahniser, M. S.; Kolb, C. E. *J. Phys. Chem.* **1991**, *95*, 6329−6336.
(4) Utter, R. G.; Burkholder, J. B.; Howard, C. J.; Ravishankara, A. R. *J. Phys. Chem.* **1992**, *96*, 4973−4979.
(5) Ponche, J. L.; George, C.; Mirabel, P. *J. Atmos. Chem.* **1993**, *16*, 1−21.
(6) Fickert, S.; Helleis, F.; Adams, J. W.; Moortgat, G. K.; Crowley, J. N. *J. Phys. Chem. A* **1998**, *102*, 10689−10696.
(7) Pöschl, U.; Canagaratna, M.; Jayne, J. T.; Molina, L. T.; Worsnop, D. R.; Kolb, C. E.; Molina, M. J. *J. Phys. Chem. A* **1998**, *102*, 10082−10089.
(8) Platz, J.; Nielsen, O. J.; Wallington, T. J.; Ball, J. C.; Hurley, M. D.; Straccia, A. M.; Schneider, W. F.; Sehested, J. *J. Phys. Chem. A* **1998**, *102*, 7964−7974.
(9) Herrmann, H.; Exner, M.; Jacobi, H. W.; Raabe, G.; Reese, A.; Zellner, R. *Faraday Discuss.* **1995**, *100*, 129−153.
(10) Herrmann, H.; Jacobi, H. W.; Raabe, G.; Reese, A.; Zellner, R. *Fresenius J. Anal.Chem.* **1996**, *355*, 343−344.
(11) vonSonntag, C. *J. Water Suppl. Res. Technol.− Aqua* **1996**, *45*, 84−91.

(12) Cencione, S. S.; Gonzalez, M. C.; Mártire, D. O. *J. Chem. Soc. Faraday Trans.* **1998**, *94*, 2933−2937.
(13) Umschlag, T.; Herrmann, H. *Acta Hydrochim. Hydrobiol.* **1999**, *27*, 214−222.
(14) Pun, B. K.; Seigneur, C.; Grosjean, D.; Saxena, P. *J. Atmos. Chem.* **1999**, *35*, 199−223.
(15) Heal, M. R.; Pilling, M. J.; Titcombe, P. E.; Whitaker, B. J. *Geophys. Res. Lett.* **1995**, *22*, 3043−3046.
(16) Leuenberger, C.; Ligocki, M. P.; Pankow, J. F. *Environ. Sci. Technol.* **1985**, *19*, 1053−1058.
(17) Levsen, K.; Behnert, S.; Priess, B.; Svoboda, M.; Winkeler, H. D.; Zietlow, J. *Chemosphere* **1990**, *21*, 1037−1061.
(18) Herterich, R.; Herrmann, R. *Environ. Technol.* **1990**, *11*, 961−972.
(19) Richartz, H.; Reischl, A.; Trautner, F.; Hutzinger, O. *Atmos. Environ.* **1990**, *24*, 3067−3071.
(20) Grosjean, D. *Sci. Total Environ.* **1991**, *100*, 367−414.
(21) Tremp, J.; Mattrel, P.; Fingler, S.; Giger, W. *Water Air Soil Pollut.* **1993**, *68*, 113−123.
(22) Lüttke, J.; Levsen, K. *Atmos. Environ.* **1997**, *31*, 2649−2655.
(23) Lüttke, J.; Levsen, K.; Acker, K.; Wieprecht, W.; Möller, D. *Int. J. Environ. Anal. Chem.* **1999**, *74*, 69−89.
(24) Schmidt-Bäumler, K.; Heberer, T.; Stan, H. J. *Acta Hydrochim. Hydrobiol.* **1999**, *27*, 143−149.
(25) Rippen, G.; Zietz, E.; Frank, R.; Knacker, T.; Klöpffer, W. *Environ. Technol. Lett.* **1987**, *8*, 475−482.
(26) Hart, K. M.; Tremp, J.; Molnar, E.; Giger, W. *Water Air Soil Pollut.* **1993**, *68*, 91−112.
(27) Natangelo, M.; Mangiapan, S.; Bagnati, R.; Benfenati, E.; Fanelli, R. *Chemosphere* **1999**, *38*, 1495−1503.
(28) Danckwerts, P. V. *Trans. Faraday Soc.* **1951**, *47*, 1014−1023.
(29) Kolb, C. E.; Worsnop, D. R.; Zahniser, M. S.; Davidovits, P.; Keyser, L. F.; Leu, M. T.; Molina, M. J.; Hanson, D. R.; Ravishankara, A. R.; Williams, L. R.; Tolbert, M. A. *Progress and Problems in Atmospheric Chemistry*; World Scientific: Singapore, 1995; Chapter 18, pp 771−875.
(30) Molina, M. J.; Molina, L. T.; Kolb, C. E. *Annu. Rev. Phys. Chem.* **1996**, *47*, 327−367.
(31) Trost, B.; Stutz, J.; Platt, U. *Atmos. Environ.* **1997**, *31*, 3999−4008.
(32) IUPAC *Summary of evaluated kinetic and photochemical data for atmospheric chemistry (Web version)*, IUPAC Subcommittee on gas kinetic data evaluation: http://www.iupac-kinetic.ch.cam.ac.uk, 2001.
(33) Bell, R. P.; Rawlinson, D. J. *J. Chem. Soc.* **1961**, 63−68.
(34) Tee, O. S.; Paventi, M.; Bennett, J. M. *J. Am. Chem. Soc.* **1989**, *111*, 2233−2240.
(35) *CRC Handbook of Chemistry and Physics*, 74th ed.; CRC Press: Boca Raton, 1993.
(36) Harrison, M. A. J.; Cape, J. N.; Heal, M. R. *Atmos. Environ.* **2002**, *36*, 1843−1851.
(37) Reid, R. C.; Prausnitz, J. M.; Poling, B. E. *The Properties of Gases and Liquids*, 4th ed.; McGraw-Hill: New York, 1987.
(38) Hanson, D. R.; Burkholder, J. B.; Howard, C. J.; Ravishankara, A. R. *J. Phys. Chem.* **1992**, *96*, 4979−4985.
(39) Davidovits, P.; Jayne, J. T.; Duan, S. X.; Worsnop, D. R.; Zahniser, M. S.; Kolb, C. E. *J. Phys. Chem.* **1991**, *95*, 6337−6340.
(40) Davidovits, P.; Hu, J. H.; Worsnop, D. R.; Zahniser, M. S.; Kolb, C. E. *Faraday Discuss.* **1995**, *100*, 65−81.
(41) Pollack, G. L. *Science* **1991**, *251*, 1323−1330.
(42) Nathanson, G. M.; Davidovits, P.; Worsnop, D. R.; Kolb, C. E. *J. Phys. Chem.* **1996**, *100*, 13007−13020.
(43) Abraham, M. H.; Andonian-Haftvan, J.; Whiting, G. S.; Leo, A.; Taft, R. S. *J. Chem. Soc.−Perkin Trans. 2* **1994**, 1777−1791.
(44) Abraham, M. H.; Du, C. M.; Platts, J. A. *J. Org. Chem.* **2000**, *65*, 7114−7118.
(45) Taylor, R. S.; Garrett, B. C. *J. Phys. Chem. B* **1999**, *103*, 844−851.
(46) Wilson, M. A.; Pohorille, A. *J. Phys. Chem. B* **1997**, *101*, 3130−3135.
(47) Maskill, H. *The physical basis of organic chemistry*; Oxford University Press: Oxford, 1990.
(48) Schwarzenbach, R. P.; Gschwend, P. M.; Imboden, D. M. *Environmental organic chemistry*; John Wiley & Sons: New York, 1993.
(49) Titcombe, P. E. Gas−liquid interactions in tropospheric chemistry. Ph.D. Thesis. School of Chemistry, University of Leeds, 1997.
(50) Schwartz, S. E. *Chemistry of multiphase atmospheric systems*; Springer-Verlag: Berlin Heidelberg, 1986; pp 415−471.
(51) Buxton, G. V.; Greenstock, C. L.; Helman, W. P.; Ross, A. B. *J. Phys. Chem. Ref. Data* **1988**, *17*, 513−886.
(52) Seinfeld, J. H.; Pandis, S. N. *Atmospheric chemistry and physics*; John Wiley & Sons: New York, 1998.
(53) Heron, G.; Christensen, T. H.; Enfield, C. G. *Environ. Sci. Technol.* **1998**, *32*, 1433−1437.
(54) *Landolt-Börnstein Physikalisch-Chemische Tabellen*, 5th ed.; Springer: Berlin, 1931.